Author Manuscript

Author Manuscript

Author Manuscript

Author Manuscript

HHS Public Access

Author manuscript

*Mol Pharm*. Author manuscript; available in PMC 2016 February 02.

Published in final edited form as:

*Mol Pharm*. 2015 February 2; 12(2): 403–410. doi:10.1021/mp500766x.

# PET of Follicle-Stimulating Hormone Receptor: Broad Applicability to Cancer Imaging

**Hao Hong**[1], **Yongjun Yan**[1,2,*], **Sixiang Shi**[3], **Stephen A. Graves**[2], **Lazura K. Krasteva**[4], **Robert J. Nickles**[2], **Min Yang**[5], and **Weibo Cai**[1,2,3,4,6,*]

[1]Department of Radiology, University of Wisconsin - Madison, Wisconsin 53705-2275, United States

[2]Department of Medical Physics, University of Wisconsin - Madison, Wisconsin 53705-2275, United States

[3]Materials Science Program, University of Wisconsin - Madison, Wisconsin 53705-2275, United States

[4]Department of Biomedical Engineering, University of Wisconsin - Madison, Wisconsin 53705-2275, United States

[5]Key Laboratory of Nuclear Medicine, Ministry of Health, Jiangsu Key Laboratory of Molecular Nuclear Medicine, Jiangsu Institute of Nuclear Medicine, Wuxi, Jiangsu, 214063, China

[6]University of Wisconsin Carbone Cancer Center, Madison, Wisconsin 53705-2275, United States

## Abstract

Selective overexpression of follicle-stimulating hormone receptor (FSHR) inside the vascular endothelium of tumors has been confirmed to play critical roles in angiogenesis, tumor invasion, and metastases. The expression level of FSHR correlates strongly with the response of tumors to antiangiogenic therapies. In this study, an immunoPET tracer was developed for imaging of FSHR in different cancer types. A monoclonal antibody (FSHR-mAb) against FSHR was conjugated with S-2-(4-isothiocyanatobenzyl)-1,4,7-triazacyclononane-1,4,7-triacetic acid (p-SCN-Bn-NOTA) and used for subsequent $^{64}$Cu-labeling. NOTA-FSHR-mAb preserved FSHR specificity/affinity, confirmed by flow cytometry measurements. $^{64}$Cu-labeling was successfully conducted with decent yields (~ 25%) and high specific activity (0.93 GBq/mg). The uptake of $^{64}$Cu-NOTA-FSHR-mAb was 3.6 ± 0.8, 13.2 ± 0.7, and 14.6 ± 0.4%ID/g in FSHR-positive CAOV-3 tumors at 4, 24, and 48 h post-injection, respectively (n = 3), significantly higher ($p<0.05$) than that in FSHR-negative SKOV-3 tumors (2.3 ± 1.2, 8.0 ± 0.9, and 9.1 ± 1.3 %ID/g at 4, 24, and 48 h post-injection, respectively (n = 3)) except at 4 h p.i. FSHR-relevant uptake of $^{64}$Cu-NOTA-FSHR-mAb was also readily observed in other tumor types (e.g. triple-negative breast tumor MDA-MB-231 or prostate tumor PC-3). Histology studies showed universal FSHR expression in

*(Y.Y.) Fax: 1-608-265-0614; Tel: 1-608-262-6153; yyan26@wisc.edu. (W.C.) Fax: 1-608-265-0614; Tel: 1-608-262-1749; wcai@uwhealth.org.

SUPPORTING INFORMATION

The internalization and efflux study results of $^{64}$Cu-NOTA-FSHR-mAb in FSHR-positive CAOV-3 cells were shown in supporting information. This material is available free of charge via the Internet at http://pubs.acs.org.

Author Manuscript Author Manuscript Author Manuscript Author Manuscript

microvasculature of these four tumor types and also prominent expression in tumor cells of CAOV-3, PC-3, and MDA-MB-231. Correlations between tumor FSHR level and uptake of $^{64}$Cu-NOTA-FSHR-mAb were witnessed in this study. FSHR-specific uptake of $^{64}$Cu-NOTA-FSHR mAb in different tumors enables its applicability for future cancer theranostic applications and simultaneously establishes FSHR as a promising clinical target for cancer.

**Keywords**

follicle-stimulating hormone receptor (FSHR); positron emission tomography (PET); molecular imaging; angiogenesis; immunoPET; Cu-64

## INTRODUCTION

As one of the major participants in both female and male reproduction,[1] follicle-stimulating hormone (FSH) is also involved in various biological events. Its receptor, FSHR, a glycosylated G-protein coupled transmembrane receptor, is expressed primarily in the granulosa cells (from the ovary) and Sertoli cells[2] (of the testicle) with detectable amount in osteoclasts and monocytes in healthy human adults.[3] In normal tissues, FSHR is only observable in placental vasculatures and ovary/testicle endothelium.[4–6] However, the abundant expression of FSHR was identified in the tumor vasculatures of a wide variety of cancers.[4, 7–10]

Although the exact pathogenic mechanism involving FSHR remains unclear, the fact that the distribution of FSHR is relatively limited in normal tissues enables its use as a targeting site for cancer detection and image-guided cancer surgery. One clinical study in cancer patients confirmed the confined FSHR expression (located between 5 mm inside the tumor and 9 mm outside the tumor), a pattern not found in healthy surrounding tissues.[4] This finding heralds new opportunities for image-guided cancer surgery. Moreover, the FSHR levels in tumors were found to correlate closely with tumor response to antiangiogenic tyrosine kinase inhibitors (e.g. sunitinib),[11] which further shows a relationship between FSHR expression and tumor angiogenesis. Besides primary tumors, elevated FSHR expression was also confirmed in the vasculature of tumor metastases.[12] Compared with “conventional” cancer imaging markers (e.g. epidermal growth factor receptor), the specificity of FSHR is higher, and FSHR-expressing endothelial cells can account for a substantial fraction inside the tumor volume (more than 60% based on the literature[4]) – these characteristics render FSHR an attractive choice for tumor detection. Moreover, the confined expression of FSHR makes it an ideal target for image-guided surgery clinically.[13]

All the aforementioned studies have established FSHR as a potential cancer theranostic target, especially for those that demonstrate resistance to regular antiangiogenic therapies. Using the FSHR-targeting strategy, a chemotherapy drug (paclitaxel, PTX)[14, 15] or a gene silencing agent (small interfering RNA, siRNA)[16] was loaded into nanoparticles which were attached to binding domains of FSH (i.e. FSH33 or FSH β 81-95). These findings underline the usefulness of FSHR-targeted nano vectors as potential delivery platforms for anticancer drugs to minimize side effects.[17]

Author Manuscript Author Manuscript Author Manuscript Author Manuscript

Despite the elucidated usefulness of FSHR in cancer detection, imaging of FSHR is currently at a comparatively preliminary stage. Only one positron emission tomography (PET) imaging study of FSHR has been reported to date.[18] In this study, FSH β 33-53 (YTRDLVYKDPARPKIQKTCTF, denoted as FSH1), a FSHR antagonist, was conjugated with NOTA and radiolabeled with [$^{18}$F] aluminum fluoride. The resulting tracer $^{18}$F-Al-NOTA-MAL-FSH1 demonstrated moderate uptake (~3 %ID/g at 0.5 h post-injection [p.i.]) in FSHR-positive PC-3 human prostate tumor xenografts with a good tumor-to-muscle ratio. However, fast washout of the tracer from the tumors and a short half-life of $^{18}$F (118 min) on the tracer limited its application in the longitudinal monitoring of FSHR expression.

Radionuclide molecular imaging techniques like PET can facilitate the monitoring of biochemical changes and target abundance within a testing subject.[19, 20] To increase the tumor uptake and retention of FSHR-targeted agents for longitudinal detection of FSHR expression levels, immunoPET imaging with radiolabeled monoclonal antibodies (mAbs) was implemented. Antibodies can offer highly selective binding and recognition of molecular targets and have motivated the identification and analysis of specific proteins for research and diagnostic purposes.[21] In this study, a mAb for FSHR (i.e. FSHR-mAb) was adopted and investigated after chelator conjugation and $^{64}$Cu-labeling for PET imaging of FSHR in different cancer models. The uptake of $^{64}$Cu-labeled FSHR-mAb in these tumors is hypothesized to correlate with their FSHR expression.

## EXPERIMENTAL SECTION

### Chemicals

FSHR-mAb was acquired from R&D Systems (MAB6559, Minneapolis, MN). Fluorescein isothiocyanate (FITC)- and Cy3-labeled secondary antibodies were purchased from Jackson Immunoresearch Laboratories, Inc. (West Grove, CA). *p*-SCN-Bn-NOTA (i.e. 2-S-(4-isothiocyanatobenzyl)-1,4,7-triazacyclononane-1,4,7-triacetic acid) was acquired from Macrocyclics, Inc. (Dallas, TX). Chelex 100 resin (50–100 mesh) was purchased from Sigma-Aldrich (St. Louis, MO). Water and all buffers were of Millipore grade and pre-treated with Chelex 100 resin to stay heavy metal-free. PD-10 columns were purchased from GE Healthcare (Piscataway, NJ). All other reaction buffers and chemicals were purchased from Thermo Fisher Scientific (Fair Lawn, NJ).

### NOTA Conjugation and $^{64}$Cu-labeling of FSHR-mAb

The reaction ratio between *p*-SCN-Bn-NOTA and FSHR-mAb was 20:1 and the conjugation procedure was conducted at pH 9.0. NOTA-FSHR-mAb was purified by PD-10 columns adopting phosphate buffered saline (PBS) as the mobile phase.

Positron-emitting copper ($^{64}$Cu) was produced with an on-site cyclotron (GE PETtrace) using a $^{64}$Ni(p,n)$^{64}$Cu reaction. A specific activity of more than 5 Ci/μmol was achieved for produced $^{64}$Cu at the end of bombardment. $^{64}CuCl_2$ (111 MBq) was diluted in 300 μL of 0.1 M sodium acetate buffer (pH 6.5) and incubated with 30 μg of FSHR-mAb at 37°C with constant shaking. After 30 min of reaction, $^{64}$Cu-NOTA-FSHR-mAb was also purified using PD-10 columns. The radioactive fractions containing $^{64}$Cu-NOTA-FSHR-mAb were passed through a 0.2 μm syringe filter prior to in vivo applications.

Author Manuscript Author Manuscript Author Manuscript Author Manuscript

### Cell FSHR-Binding Assays

In vitro FSHR-binding affinity of NOTA-FSHR-mAb was evaluated by cell binding assay (utilizing compound displacement on the receptor) using $^{64}$Cu-NOTA-FSHR-mAb as the FSHR-specific radioligand. Experiments were performed on CAOV-3 cells by a previously described procedure.[22] The 50% inhibitory concentration ($IC_{50}$) values for CAOV-3 cells were calculated by nonlinear regression with GraphPad Prism (v 6.05, GraphPad Software, Inc.). Triplicate sampling was used for all the experiments.

### Flow Cytometry

The binding affinity of FSHR-mAb and its NOTA conjugates for FSHR was evaluated in CAOV-3 human ovarian cancer cells (FSHR-positive) and SKOV-3 human ovarian cancer cells (FSHR-negative).[14] Cells were resuspended in cold PBS (supplemented with 2% bovine serum albumin) to a final concentration of 5 million cells per milliliter. After incubation with FSHR-mAb or NOTA-FSHR-mAb (5 μg/mL) for 0.5 h at room temperature, the cells were washed thrice with cold PBS. FITC-labeled rabbit anti-mouse IgG (1 μg/mL) was then added into the cell suspensions for further incubation of 0.5 h (at room temperature). After the final washing with cold PBS (thrice), the cells were analyzed using a BD FACSCalibur 4-color analysis cytometer, equipped with 488 nm and 633 nm lasers (Becton-Dickinson, San Jose, CA). FlowJo (Tree Star, Inc., Ashland, OR) was used to calculate the fluorescence distributions of the cells.

### Tumor-bearing Mouse Model

All animal studies were conducted in compliance with the regulations by University of Wisconsin Institutional Animal Care and Use Committee. For tumor establishment, 5 million of CAOV-3 (FSHR-positive[14]), SKOV-3 (FSHR-negative[14]), PC-3 (FSHR-positive[18]), or MDA-MB-231 cells (FSHR-positive) suspended in 100 μL of a 1:1 mixture of PBS and Matrigel (BD Biosciences, Franklin lakes, NJ) was subcutaneously injected into the front flank of male nude mice (Harlan, Indianapolis, IN). The tumor sizes were monitored twice per week and the mice were subjected to in vivo experiments when the tumor diameter reached 6–8 mm (angiogenesis is very active at this stage).

### PET Imaging and Biodistribution Studies

An Inveon microPET/microCT (Siemens Medical Solutions USA, Inc.) was used for PET scanning. Each tumor-bearing mouse was injected with 5–10 MBq of $^{64}$Cu-NOTA-FSHR-mAb via tail vein and subjected to 5–15 minutes of static PET scans at different chosen time points p.i. Maximum a posteriori (MAP) algorithm was chosen for image reconstruction, adopting no attenuation or scatter correction. Inveon research workshop (IRW) was used to superimpose three-dimensional (3D) regions-of-interest (ROIs) on the tumor and major organs in the decay-corrected whole-body images. The radioactivity in each ROI volume was converted to MBq/g and then divided by the total administered radioactivity to obtain a percentage of injected dose per gram of tissue (%ID/g) for each ROI.

After the last PET scans at 48 h p.i., the mice were euthanized and their blood, CAOV-3/SKOV-3/PC-3/MDA-MB-231 tumors, and major organs/tissues were collected and wet-

Author Manuscript Author Manuscript Author Manuscript Author Manuscript

weighed. The radioactivity in each collected sample was measured using a WIZARD$^2$ automatic gamma-counter (Perkin Elmer) and recorded as %ID/g (mean ± SD).

### Histology

Tissues were cut into frozen slices of 5 μm thickness and fixed with cold acetone for 10 min and air dried in the laboratory for 0.5 h. The slices were incubated with FSHR-mAb (5 μg/mL) post PBS rinse and blocking with 10% donkey serum for 30 min at room temperature. After a 1 h incubation at 4 °C, the tissue slices were repeatedly rinsed by PBS and visualized by FITC-labeled rabbit anti-mouse secondary antibody. The tissue slices were also stained for endothelial marker CD31 with a rat anti-mouse CD31 antibody (Clone: MEC13.3, BD Biosciences, 1:50 dilution with PBS) for 1 h, followed by Cy3-labeled donkey anti-rat IgG (2 μg/mL) for 30 min. All fluorescence images were taken with a Nikon Eclipse Ti microscope.

### Quantitative real time RT-PCR

The total RNA was isolated from tumors (without separation of tumor cells from tumor vasculature in order to compare with PET imaging results) after the decay of radioactivity. Tumors were snap frozen by liquid nitrogen, immersed in a RNA later buffer, and subjected to homogenization. RNA was extracted using Qiagen RNeasy Minikit (Qiagen Inc., Valencia, CA), reversely transcribed, and amplified using Qiagen OneStep RT-PCR kit. Real-time PCR was performed using TaqMan primers for FSHR (Hs00174865_m1 Fshr) and GAPDH (Mm99999915_g1 Gapdh) (Applied Biosystems, Carslbad, CA). Ct (threshold cycle) values from real-time PCR were used for the quantification of FSHR and GAPDH expression. PCR products were run on 1% agarose gel under the condition of 100 V/1 h.

### Statistical Analysis

Data were presented in the format of mean ± SD. Means were compared using Student's t-test. P values $< 0.05$ were considered statistically significant.

## RESULTS

### In vitro investigation of NOTA-FSHR-mAb

CAOV-3 cell (which expressed high levels of FSHR) FSHR-binding assay revealed that the $IC_{50}$ value was 13.1 ± 1.3 nM for NOTA-FSHR-mAb (Figure 1A). Data from flow cytometry analysis in CAOV-3 confirmed comparable binding affinities for FSHR between FSHR-mAb and NOTA-FSHR-mAb. Antigen specific binding to CAOV-3 was confirmed as both FSHR-mAb and NOTA-FSHR-mAb demonstrated minimal interaction with FSHR-negative SKOV-3 cells (Figure 1B). Together, these findings indicated that NOTA-FSHR-mAb has good affinity and specificity to FSHR. The cellular efflux studies of $^{64}$Cu-NOTA-FSHR-mAb in CAOV-3 cells indicated that significant amount (over 40%) of radiolabeled antibody was excreted from the cells within 3 hours post-incubation (Supplemental Figure 1).

Author Manuscript Author Manuscript Author Manuscript Author Manuscript

## Radiolabeling and PET imaging

The $^{64}$Cu-labeling procedure could be completed in a time frame of 100 ± 10 min (n = 8). With decay correction, the radiochemical yields in this study were 25 ± 9 %, calculated from the reaction ratio (10 μg of NOTA-FSHR-mAb per 37 MBq of $^{64}CuCl_2$). A specific activity of 0.93 GBq/mg protein was acquired for $^{64}$Cu-NOTA-FSHR-mAb.

Drawing on prior experiences in PET imaging with $^{64}$Cu-labeled antibodies,[23–25] 4, 24, and 48 h p.i. were chosen for serial PET scans. Coronal PET slices that included the CAOV-3, SKOV-3, PC-3 or MDA-MB-231 tumors are shown in Figure 2. ROI quantification analysis for each time point are presented in Figure 3. Blood pool activity was prominent at both 4 h and 24 h p.i. and gradually declined at 48 h p.i. (Table 1). The same trend was displayed in the liver uptake of $^{64}$Cu-NOTA-FSHR-mAb in CAOV-3 tumor-bearing mice. The uptake of $^{64}$Cu-NOTA-FSHR-mAb in CAOV-3 tumors climbed considerably from 4 h p.i. (tumor was also clearly visible at that time) and plateaued from around 24 h p.i. (Table 1 and Figure 3A).

The SKOV-3 tumor, which expresses a significantly lower level of FSHR, was selected as a control here. A significantly lower uptake of $^{64}$Cu-NOTA-FSHR-mAb was observed in SKOV-3 at 24 and 48 h p.i. ($p<0.05$, Table 1 and Figure 3B). Similar liver uptake and the blood radioactivity (Table 1 and Figure 3B) were confirmed when compared with those in the CAOV-3 tumor model. Compared with these two tumors, MDA-MB-231 and PC-3 tumors also demonstrated medium and high level uptake of the tracer (Table 1 and Figure 3C&D). The liver uptake and the blood radioactivity (Table 1 and Figure 3C&D) were similar to those in the CAOV-3 or SKOV-3 tumor model.

## Biodistribution studies

Significant radioactivity accumulation was observed in tumors, liver, spleen, and blood from the tumor-bearing mice at 48 h p.i., an expected result coming from the long circulation half-life and hepatic clearance of $^{64}$Cu-NOTA-FSHR-mAb (Figure 4). Recognizable radioactivity (~5 %ID/g) in the kidney was also observed, possibly due to partial $^{64}$Cu detachment from NOTA-FSHR-mAb and the degradation of FSHR-mAb over time. Apart from the tumors, $^{64}$Cu-NOTA-FSHR-mAb demonstrated a similar distribution profile in all the other major organs/tissues from all four types of tumor-bearing mice. Uptake of $^{64}$Cu-NOTA-FSHR-mAb in the CAOV-3 tumor was significantly higher than in the SKOV-3 or PC-3 model but comparable to that in MDA-MB-231 tumor. An excellent tumor contrast was achieved for $^{64}$Cu-NOTA-FSHR-mAb in CAOV-3 tumor bearing mice with a tumor/muscle ratio of 27.5 ± 3.4 at 48 h p.i. (n = 3).

## Histology and RT-PCR

Prominent FSHR expression was confirmed by Immunofluorescence FSHR/CD31 staining on both tumor cells and the tumor vasculature of CAOV-3 and MDA-MB-231, and FSHR existence was only observable on the SKOV-3 vasculature (Figure 5A). On the other hand, PC-3 demonstrated a high level of FSHR on its vasculature. A significant amount of PC-3 tumor cells were also identified as FSHR-positive, but the expression level was lower than that from CAOV-3 and MDA-MB-231.

Author Manuscript Author Manuscript Author Manuscript Author Manuscript

Linear correlation was confirmed between the $^{64}$Cu-NOTA-FSHR-mAb uptake at 48 h p.i. and FSHR level from whole tumors measured by RT-PCR (indicated by FSHR/GAPDH ratio, $r^2 = 0.88$, $P<0.001$, Figure 5B). Since the expression level of FSHR was normalized to GAPDH, the excellent linear correlation suggests that the uptake of $^{64}$Cu-NOTA-FSHR-mAb reflects the accurate FSHR expression level in vivo. In addition, the fluorescence intensities from different tumor histological slides (n = 5 for each tumor types) were quantified by ImageJ (1.48v, National Institutes of Health) and demonstrated a similar linear relationship to according tumor uptakes of $^{64}$Cu-NOTA-FSHR-mAb ($r^2 = 0.73$, $P<0.01$, Figure 5B).

## DISCUSSION

FSH and FSHR play a critical role in mammalian reproduction via their specific interaction.[2, 26, 27] The interactions between FSH and FSHR trigger adenylyl cyclase activation and cAMP production, which follows by elevation of intracellular $Ca^{2+}$ concentration and protein kinase A (PKA) activation, eventually initiating a series of downstream protein networks.[7, 9, 10] More importantly, FSHR is primarily expressed in the tumor associated endothelial cells.[4, 28–30] From the initial report confirming universal FSHR expression in the tumor endothelium, over one thousand primary tumors from 11 categories were evaluated by histology and immunoblotting examination.[4] Certain tumor cells (e.g. breast, prostate, or pancreatic) could also be faintly stained by FSHR antibodies, but no clear pattern was established. The confined expression pattern of FSHR in tumor tissues is one of its advantages for tumor detection/treatment compared with other established tumor markers,[4] which bestows FSHR-targeting agents high clinical relevance. Despite its important role in tumor angiogenesis and progression, not enough information has been collected on molecular mechanisms of how FSHR participates in tumorigenesis and growth stimulation. Semiquantitative RT-PCR was previously carried out to assess the cellular FSHR mRNA level,[31] but for the monitoring of FSHR expression in vivo, more delicate and reliable tools will be needed.

Molecular imaging, on the other hand, has a tremendous capacity to provide the visualization and characterization of FSHR-related molecular and cellular events in vivo.[32] Among all of the molecular imaging modalities, nuclear imaging techniques including SPECT and PET can provide sensitive (down to the $10^{-12}$ M) and quantitative detection of biological events with no tissue penetration limit.[33] A series of clinical data have supported the great potential of immunoPET for cancer patients management.[21] Antibody-based tracers possess good target specificity and binding affinity, which enable them to have a strong absolute accumulation in the tumor. These characteristics render them suitability to be used in internal radiotherapy and/or for delivery efficiency enhancement of anti-cancer drugs. On the other hand, slow tumor penetration and nonspecific absorption in the reticuloendothelial system are primary limiting factors for antibody-based imaging agents. To date there is only report of using $^{18}$F-labeled FSH peptidic fragments for imaging of FSHR in vivo.[18] Although significant tumor uptake (~ 3%ID/g) could be observed in this study at early time points (30 min p.i.), low stability and fast wash-out of this peptide tracer from tumor was the major limitation of this study. Compared with that, the $^{64}$Cu-labeled FSHR-mAb used in the current study possesses higher affinity for FSHR and higher stability

Author Manuscript Author Manuscript Author Manuscript Author Manuscript

in vivo (> 10%ID/g uptake observable at 48 h p.i.), thus making it more suitable for long-term monitoring of FSHR fluctuation during tumor progression in vivo.

In this study, we adopted a $^{64}$Cu-labeled FSHR antibody ($^{64}$Cu-NOTA-FSHR-mAb) for PET imaging of tumor FSHR abundance. At the current stage, we cannot discriminate FSHR expression on tumor cells (e.g. CAOV-3) from the surrounding vascular endothelium – we speculate that both of FSHR will be imaged by $^{64}$Cu-NOTA-FSHR-mAb developed in this study. The main advantages of $^{64}$Cu-NOTA-FSHR-mAb are its strong and specific binding to FSHR in vivo, which brings out prominent accumulation in the tumor. Cancer cells with different FSHR expression were chosen according to previous reports[14, 18] and confirmed by FACS, RT-PCR, or immunohistological examination. The FSHR binding characteristics of FSHR-mAb and NOTA-FSHR-mAb were evaluated in this study and the acquired data demonstrated no significant loss of the FSHR binding affinity after NOTA conjugation. Consistent with our hypothesis, $^{64}$Cu-NOTA-FSHR-mAb had higher accumulation in FSHR-positive CAOV-3/MDA-MB-231/PC-3 tumors. Although the uptake of $^{64}$Cu-NOTA-FSHR-mAb in FSHR-negative SKOV-3 was still noticeable, it is largely related to the vasculature expression of FSHR, which was confirmed by immunohistological staining. The FSHR on tumor endothelial cells should be more accessible to FSHR-mAb since it will take time for FSHR-mAb to penetrate and interact with tumor cells. That could potentially account for the fast accumulation of $^{64}$Cu-NOTA-FSHR-mAb in tumor at early time points (4 h p.i.). In summary, the tumor uptake of $^{64}$Cu-NOTA-FSHR-mAb correlated closely with the FSHR expression levels. Such in vivo FSHR specificity enables the broad applicability of $^{64}$Cu-NOTA-FSHR-mAb as a PET tracer in various clinical applications. The long-term behavior of FSHR-mAb can be explored in future studies by adoption of long-lived isotopes (e.g., $^{89}$Zr, $t_{1/2}$ = 78.4 h[34]).

The traveling of $^{64}$Cu rather than the antibody itself is detected by PET scanners, so in order to acquire accurate PET data, the $^{64}$Cu-labeled antibodies should be sufficiently stable, at least within the monitoring time frame. The reason we chose NOTA as the $^{64}$Cu labeling chelator in this study is that it is considered as one of the strongest and most stable coordinating compound for $^{64}$Cu. One recent study investigated the impacts of $^{64}$Cu chelators on the biodistribution of radiolabeled antibodies,[35] and they came to the conclusion that the stability of $^{64}$Cu-chelator complexes primarily affected the absorption of radiolabeled antibodies in normal tissues – they had little influence on tracer's tumor uptake.

The discovery of FSHR overexpression in primary and metastatic cancer[9, 12] provided an invaluable opportunity for cancer theranostics using this target. The expression of FSHR was identified in various cancer types which have different surface receptor profiles and variable malignant behavior, indicating that detection sensitivity based on FSHR will not be influenced by tumor phenotype and behavior heterogeneity. The specificity of this target is very high, as the FSHR is confirmed to be expressed only on granulosa cells or Sertoli cells in adult humans.[2] Although the amount of FSHR is lower in smaller tumors, researchers have confirmed that FSHR-expressing endothelial cells also account for a substantial percentage of the total tumor mass.[4] One potential drawback of FSHR-targeting is that this tumor identification strategy is only feasible following the formation of tumor blood vessels after the angiogenic switch is on. However, tumor volume is usually limited to 2–3 mm$^3$ in

Author Manuscript Author Manuscript Author Manuscript Author Manuscript

the prevascular phase and considered as clinically undetectable by modern detection methods.[36] Similar to other growth factor receptors targeting molecules, certain contrast agents for FSHR can cause potentially detrimental effects (e.g. the trigger of tumor proliferation). A monoclonal antibody was used in this study instead of FSH peptide sequences, and the application concentration of $^{64}$Cu-NOTA-FSHR-mAb was lower than the nanomolar range, which minimized the contribution of the tracer to changes in FSHR expression.

Blocking studies were not undertaken with radiolabeled FSHR-mAb due to the limited quantity of this antibody. However, combined with different in vitro and ex vivo validation, we confirmed the feasibility of $^{64}$Cu-NOTA-FSHR-mAb PET for assessment of FSHR expression. The expression of the FSHR provides an optimal cancer imaging target and could theoretically circumvent the problems of tumor heterogeneity.[13] Moreover, the inability to identify individual invasive tumor strands requires a new approach to consistently include an objective resection margin into the surgical resection. The FSHR positive margin would provide such a consistent objective resection margin. Compared with other radioactive molecules for cancer diagnosis, $^{64}$Cu-NOTA-FSHR-mAb possesses several benefits: it targets an easily accessible marker with high specificity, it works for both primary and metastatic tumors, and it can be used for both tumor detection and surgical removal guidance. These unique benefits make it readily transferrable into a clinical scenario.

## CONCLUSION

The characterization and in vivo investigation of $^{64}$Cu-labeled FSHR-mAb was reported here in mouse tumor models with different expression levels of FSHR. $^{64}$Cu-NOTA-FSHR-mAb exhibited FSHR-specific uptake in various tumors. After further pharmacokinetic evaluation and dose optimization, $^{64}$Cu-NOTA-FSHR-mAb can be a promising candidate for future FSHR-targeted cancer therapy or image-guided surgery in clinics.

## Supplementary Material

Refer to Web version on PubMed Central for supplementary material.

## Acknowledgments

This work is supported, in part, by the University of Wisconsin - Madison Department of Radiology and Medical Physics (R&D Award 1105-002), the National Institutes of Health (NIBIB/NCI 1R01CA169365 and P30CA014520), the Department of Defense (W81XWH-11-1-0644), the American Cancer Society (125246-RSG-13-099-01-CCE), and the National Natural Science Foundation of China (81171399 and 81101077).

## References

1. Tapanainen JS, Aittomaki K, Min J, Vaskivuo T, Huhtaniemi IT. Men homozygous for an inactivating mutation of the follicle-stimulating hormone (FSH) receptor gene present variable suppression of spermatogenesis and fertility. Nat Genet. 1997; 15:205–6. [PubMed: 9020851]
2. Simoni M, Gromoll J, Nieschlag E. The follicle-stimulating hormone receptor: biochemistry, molecular biology, physiology, and pathophysiology. Endocr Rev. 1997; 18:739–73. [PubMed: 9408742]

Author Manuscript Author Manuscript Author Manuscript Author Manuscript


3. Robinson LJ, Tourkova I, Wang Y, Sharrow AC, Landau MS, Yaroslavskiy BB, Sun L, Zaidi M, Blair HC. FSH-receptor isoforms and FSH-dependent gene transcription in human monocytes and osteoclasts. Biochem Biophys Res Commun. 2010; 394:12–7. [PubMed: 20171950]
4. Radu A, Pichon C, Camparo P, Antoine M, Allory Y, Couvelard A, Fromont G, Hai MT, Ghinea N. Expression of follicle-stimulating hormone receptor in tumor blood vessels. N Engl J Med. 2010; 363:1621–30. [PubMed: 20961245]
5. Vannier B, Loosfelt H, Meduri G, Pichon C, Milgrom E. Anti-human FSH receptor monoclonal antibodies: immunochemical and immunocytochemical characterization of the receptor. Biochemistry. 1996; 35:1358–66. [PubMed: 8634264]
6. Vu Hai MT, Lescop P, Loosfelt H, Ghinea N. Receptor-mediated transcytosis of follicle-stimulating hormone through the rat testicular microvasculature. Biol Cell. 2004; 96:133–44. [PubMed: 15050368]
7. Parrott JA, Doraiswamy V, Kim G, Mosher R, Skinner MK. Expression and actions of both the follicle stimulating hormone receptor and the luteinizing hormone receptor in normal ovarian surface epithelium and ovarian cancer. Mol Cell Endocrinol. 2001; 172:213–22. [PubMed: 11165055]
8. Ferlin A, Pengo M, Selice R, Salmaso L, Garolla A, Foresta C. Analysis of single nucleotide polymorphisms of FSH receptor gene suggests association with testicular cancer susceptibility. Endocr Relat Cancer. 2008; 15:429–37. [PubMed: 18430895]
9. Gartrell BA, Tsao CK, Galsky MD. The follicle-stimulating hormone receptor: a novel target in genitourinary malignancies. Urol Oncol. 2013; 31:1403–7. [PubMed: 22513137]
10. Gloaguen P, Crepieux P, Heitzler D, Poupon A, Reiter E. Mapping the follicle-stimulating hormone-induced signaling networks. Front Endocrinol (Lausanne). 2011; 2:45. [PubMed: 22666216]
11. Siraj MA, Pichon C, Radu A, Ghinea N. Endothelial follicle stimulating hormone receptor in primary kidney cancer correlates with subsequent response to sunitinib. J Cell Mol Med. 2012; 16:2010–6. [PubMed: 22129368]
12. Siraj A, Desestret V, Antoine M, Fromont G, Huerre M, Sanson M, Camparo P, Pichon C, Planeix F, Gonin J, Radu A, Ghinea N. Expression of follicle-stimulating hormone receptor by the vascular endothelium in tumor metastases. BMC Cancer. 2013; 13:246. [PubMed: 23688201]
13. Keereweer S, Van Driel PB, Robinson DJ, Lowik CW. Shifting focus in optical image-guided cancer therapy. Mol Imaging Biol. 2014; 16:1–9. [PubMed: 24037176]
14. Zhang XY, Chen J, Zheng YF, Gao XL, Kang Y, Liu JC, Cheng MJ, Sun H, Xu CJ. Follicle-stimulating hormone peptide can facilitate paclitaxel nanoparticles to target ovarian carcinoma in vivo. Cancer Res. 2009; 69:6506–14. [PubMed: 19638590]
15. Zhang X, Chen J, Kang Y, Hong S, Zheng Y, Sun H, Xu C. Targeted paclitaxel nanoparticles modified with follicle-stimulating hormone beta 81-95 peptide show effective antitumor activity against ovarian carcinoma. Int J Pharm. 2013; 453:498–505. [PubMed: 23811008]
16. Hong S, Zhang X, Chen J, Zhou J, Zheng Y, Xu C. Targeted gene silencing using a follicle-stimulating hormone peptide-conjugated nanoparticle system improves its specificity and efficacy in ovarian clear cell carcinoma in vitro. J Ovarian Res. 2013; 6:80. [PubMed: 24252539]
17. Modi DA, Sunoqrot S, Bugno J, Lantvit DD, Hong S, Burdette JE. Targeting of follicle stimulating hormone peptide-conjugated dendrimers to ovarian cancer cells. Nanoscale. 2014; 6:2812–20. [PubMed: 24468839]
18. Xu Y, Pan D, Zhu C, Xu Q, Wang L, Chen F, Yang R, Luo S, Yang M, Yan Y. Pilot Study of a Novel $^{18}$F-labeled FSHR Probe for Tumor Imaging. Mol Imaging Biol. 2014; 16:578–85. [PubMed: 24389931]
19. Holland JP, Cumming P, Vasdev N. PET radiopharmaceuticals for probing enzymes in the brain. Am J Nucl Med Mol Imaging. 2013; 3:194–216. [PubMed: 23638333]
20. James ML, Gambhir SS. A molecular imaging primer: modalities, imaging agents, and applications. Physiol Rev. 2012; 92:897–965. [PubMed: 22535898]
21. Wu AM. Antibodies and antimatter: the resurgence of immuno-PET. J Nucl Med. 2009; 50:2–5. [PubMed: 19091888]

Author Manuscript Author Manuscript Author Manuscript Author Manuscript

22. Yang Y, Niu Y, Hong H, Wu H, Zhang Y, Engle JW, Barnhart TE, Cai J, Cai W. Radiolabeled gamma-AApeptides: a new class of tracers for positron emission tomography. Chem Comm. 2012; 48:7850–2. [PubMed: 22785080]
23. Hong H, Yang Y, Zhang Y, Engle JW, Barnhart TE, Nickles RJ, Leigh BR, Cai W. Positron emission tomography imaging of CD105 expression during tumor angiogenesis. Eur J Nucl Med Mol Imaging. 2011; 38:1335–43. [PubMed: 21373764]
24. Hong H, Zhang Y, Nayak TR, Engle JW, Wong HC, Liu B, Barnhart TE, Cai W. Immuno-PET of tissue factor in pancreatic cancer. J Nucl Med. 2012; 53:1748–54. [PubMed: 22988057]
25. Zhang Y, Hong H, Engle JW, Yang Y, Barnhart TE, Cai W. Positron Emission Tomography and Near-Infrared Fluorescence Imaging of Vascular Endothelial Growth Factor with Dual-Labeled Bevacizumab. Am J Nucl Med Mol Imaging. 2012; 2:1–13. [PubMed: 22229128]
26. Dierich A, Sairam MR, Monaco L, Fimia GM, Gansmuller A, LeMeur M, Sassone-Corsi P. Impairing follicle-stimulating hormone (FSH) signaling in vivo: targeted disruption of the FSH receptor leads to aberrant gametogenesis and hormonal imbalance. Proc Natl Acad Sci U S A. 1998; 95:13612–7. [PubMed: 9811848]
27. Lalioti MD. Impact of follicle stimulating hormone receptor variants in fertility. Curr Opin Obstet Gynecol. 2011; 23:158–67. [PubMed: 21372710]
28. Yang CQ, Chan KY, Ngan HY, Khoo US, Chiu PM, Chan QK, Xue WC, Cheung AN. Single nucleotide polymorphisms of follicle-stimulating hormone receptor are associated with ovarian cancer susceptibility. Carcinogenesis. 2006; 27:1502–6. [PubMed: 16574671]
29. Ji Q, Liu PI, Chen PK, Aoyama C. Follicle stimulating hormone-induced growth promotion and gene expression profiles on ovarian surface epithelial cells. Int J Cancer. 2004; 112:803–14. [PubMed: 15386376]
30. Bose CK. Follicle stimulating hormone receptor (FSHR) antagonist and epithelial ovarian cancer (EOC). J Exp Ther Oncol. 2007; 6:201–4. [PubMed: 17552360]
31. Syed V, Ulinski G, Mok SC, Yiu GK, Ho SM. Expression of gonadotropin receptor and growth responses to key reproductive hormones in normal and malignant human ovarian surface epithelial cells. Cancer Res. 2001; 61:6768–76. [PubMed: 11559549]
32. Mankoff DA. A definition of molecular imaging. J Nucl Med. 2007; 48:18N, 21N.
33. Gambhir SS. Molecular imaging of cancer with positron emission tomography. Nat Rev Cancer. 2002; 2:683–93. [PubMed: 12209157]
34. Hong H, Severin GW, Yang Y, Engle JW, Zhang Y, Barnhart TE, Liu G, Leigh BR, Nickles RJ, Cai W. Positron emission tomography imaging of CD105 expression with $^{89}$Zr-Df-TRC105. Eur J Nucl Med Mol Imaging. 2012; 39:138–48. [PubMed: 21909753]
35. Dearling JL, Voss SD, Dunning P, Snay E, Fahey F, Smith SV, Huston JS, Meares CF, Treves ST, Packard AB. Imaging cancer using PET--the effect of the bifunctional chelator on the biodistribution of a $^{64}$Cu-labeled antibody. Nucl Med Biol. 2011; 38:29–38. [PubMed: 21220127]
36. Folkman J. Angiogenesis in cancer, vascular, rheumatoid and other disease. Nat Med. 1995; 1:27–31. [PubMed: 7584949]

Author Manuscript Author Manuscript Author Manuscript Author Manuscript

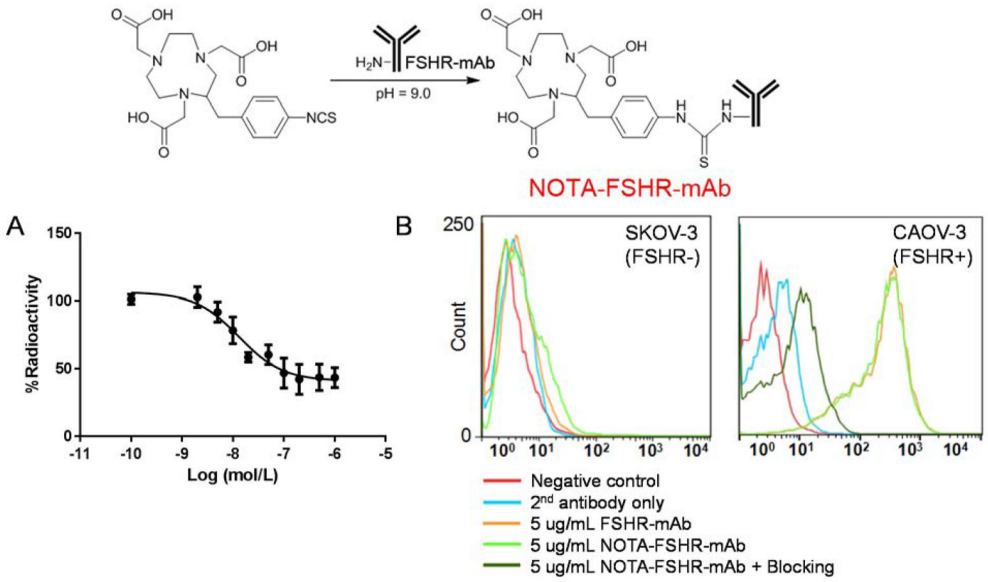


**Figure 1.**

NOTA conjugation scheme and FSHR-binding affinity analysis of FSHR-mAb. (A) Cell binding curve of $^{64}$Cu-NOTA-FSHR-mAb in CAOV-3 (FSHR-positive) cells with competition of FSHR-mAb at different concentrations. (B) Flow cytometry analysis of FSHR-mAb and NOTA-FSHR-mAb in CAOV-3 (FSHR-positive) and SKOV-3 (FSHR-negative) cells at the concentration of 5 μg/mL. 50 μg of FSHR-mAb was used in the blocking group.

Author Manuscript Author Manuscript Author Manuscript Author Manuscript

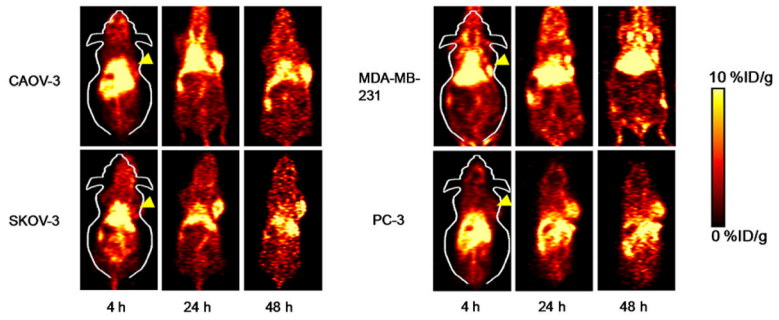


**Figure 2.**

Serial PET imaging of FSHR in CAOV-3, SKOV-3, MDA-MB-231, and PC-3 tumor-bearing mice. Serial coronal PET images of tumor-bearing mice at 4, 24, and 48 h post-injection of $^{64}$Cu-NOTA-FSHR-mAb were demonstrated.

Author Manuscript Author Manuscript Author Manuscript Author Manuscript

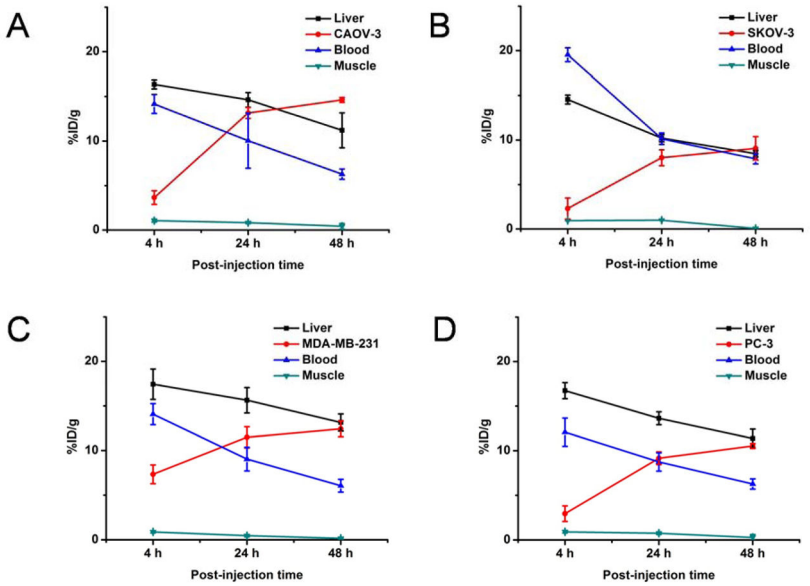


**Figure 3.**

Time-activity curves of the tumor, liver, blood, and muscle upon intravenous injection of $^{64}$Cu-NOTA-FSHR-mAb into CAOV-3 (A), SKOV-3 (B), MDA-MB-231 (C), and PC-3 (D) tumor-bearing mice (n = 3).

Author Manuscript Author Manuscript Author Manuscript Author Manuscript

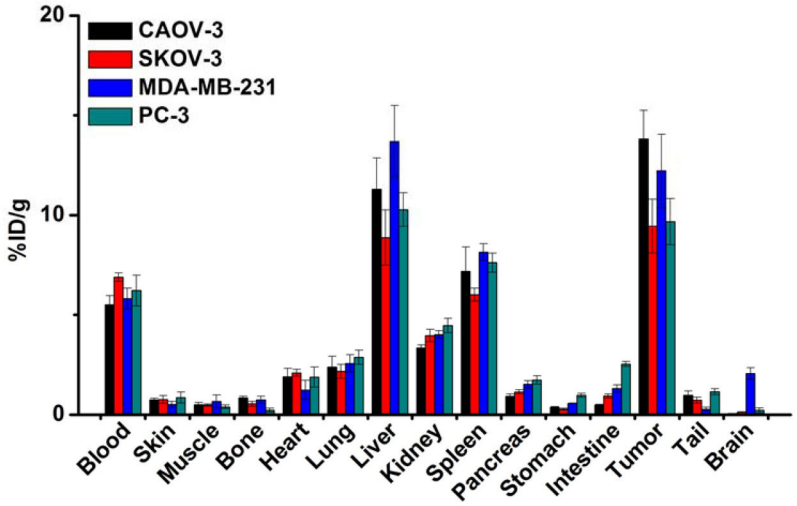


**Figure 4.**

Biodistribution of $^{64}$Cu-NOTA-FSHR-mAb in CAOV-3, SKOV-3, MDA-MB-231, and PC-3 tumor-bearing mice at 48 h post-injection (n = 3).

Author Manuscript Author Manuscript Author Manuscript Author Manuscript

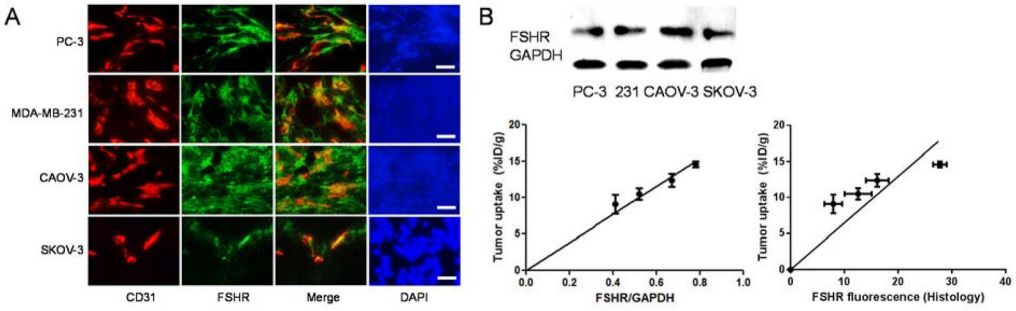


**Figure 5.**

Ex vivo examination of FSHR expression. (A) Immunofluorescence FSHR/CD31 double-staining of the CAOV-3, SKOV-3, MDA-MB-231, and PC-3 tumor sections. FSHR-mAb and FITC-labeled goat anti-mouse IgG were used for FSHR staining (green). Subsequently, the tissue slices were stained with rat anti-mouse CD31 antibody and Cy3-labeled donkey anti-rat IgG (red). All images were acquired under the same conditions and are displayed on the same scale. Scale bar: 50 μm. The FSHR fluorescence-tumor uptake correlation curve was also given here with the quantification of fluorescence by ImageJ. (B) RT-PCR assessment of FSHR expression in different tumors. FSHR expression in different tumors was visualized in 1% agarose gel by ethidium bromide. Correlation of relative tumor tissue FSHR expression (via FSHR/GAPDH ratio) and the average %ID/g values of tumor $^{64}$Cu-NOTA-FSHR-mAb uptake (measured by PET) at 48 h p.i. was also shown.

Author Manuscript

Author Manuscript

Author Manuscript

Author Manuscript

**Table 1**

The uptake of $^{64}$Cu-NOTA-FSHR-mAb in different tissues based on ROI analysis (n = 3)

| | Tumor (%ID/g) | Liver (%ID/g) | Blood (%ID/g) | Muscle (%ID/g) |
|---|---|---|---|---|
| **4 h p.i.** | | | | |
| **CAOV-3** | 3.6 ± 0.8 | 16.4 ± 0.5 | 14.2 ± 1.1 | 1.0 ± 0.2 |
| **SKOV-3** | 2.3 ± 1.2 | 14.5 ± 0.9 | 19.5 ± 0.7 | 0.9 ± 0.01 |
| **MDA-MB-231** | 7.3 ± 1.0 | 17.4 ± 1.7 | 14.1 ± 1.2 | 0.9 ± 0.1 |
| **PC-3** | 2.9 ± 0.9 | 16.7 ± 1.4 | 12.1 ± 1.6 | 0.9 ± 0.1 |
| **24 h p.i.** | | | | |
| **CAOV-3** | 13.2 ± 0.7 | 14.6 ± 0.8 | 10.0 ± 3.0 | 0.8 ± 0.1 |
| **SKOV-3** | 8.0 ± 0.9 | 10.2 ± 0.6 | 10.1 ± 0.6 | 0.9 ± 0.03 |
| **MDA-MB-231** | 11.5 ± 1.2 | 15.6 ± 1.4 | 9.0 ± 1.3 | 0.5 ± 0.1 |
| **PC-3** | 9.1 ± 0.7 | 13.6 ± 0.7 | 8.7 ± 1.0 | 0.8 ± 0.2 |
| **48 h p.i.** | | | | |
| **CAOV-3** | 14.6 ± 0.4 | 11.2 ± 2.0 | 6.3 ± 0.6 | 0.4 ± 0.2 |
| **SKOV-3** | 9.1 ± 1.3 | 8.5 ± 0.4 | 7.9 ± 0.6 | 0.1 ± 0.02 |
| **MDA-MB-231** | 12.4 ± 0.9 | 13.1 ± 1.0 | 6.1 ± 0.7 | 0.2 ± 0.04 |
| **PC-3** | 10.5 ± 0.8 | 11.3 ± 1.0 | 6.3 ± 0.6 | 0.3 ± 0.2 |